C. Brillante, M. Morandini, P. Mantegazza
Periodic Controllers for Vibration Reduction Using Actively Twisted Blades
The Aeronautical Journal, Vol. 120, N. 1233, 2016, p. 1763-1784
doi:10.1017/aer.2016.80

Page 1 of 18. © Royal Aeronautical Society

Periodic controllers for vibration reduction using actively twisted blades

Claudio Brillante
claudio.brillante@mail.polimi.it

Dipartimento di Scienze e Tecnologie Aerospaziali
Politecnico di Milano
Milano
Italy

Marco Morandini*
marco.morandini@polimi.it

Dipartimento di Scienze e Tecnologie Aerospaziali
Politecnico di Milano
Milano
Italy

Paolo Mantegazza
paolo.mantegazza@polimi.it

Dipartimento di Scienze e Tecnologie Aerospaziali
Politecnico di Milano
Milano
Italy

Keywords: Active twist rotor, periodic control, vibration control, free wake.

ABSTRACT

This paper compares two periodic control methods, the optimal H_2 and the periodic static output feedback (POF), to reduce the helicopter rotor vibrations. Actively twisted blades with macro-fiber composite (MFC) piezoelectric actuators are used. The design model is based on a simplified aerodynamic model and on a multibody model of the Bo105 isolated rotor with the original blades replaced by actively twisted ones. The performance of the two controllers in alleviating hub loads is verified with improved simulations based on a free wake model.

* Corresponding author

.

NOMENCLATURE

c	Blade choord
A_k, B_k, C_k, D_k	Discrete time model matrices
A_k^C, B_k^C, C_k^C, D_k^C	Periodic controlle matrices
C_L, C_D, C_M	Lift, drag and moment coefficients
C_nM^2	Sectional normal force coefficient
$E\{.,.\}$	Variance matrix
$E[.]$	Expected value
F	Tip loss correction factor
F_z	Blade root shear force
F_Z	Hub vertical force
J	Performance index
K_k	Feedback proportional gain
M_X, M_Y	Hub moment along x and y axis
N	Discrete controller period
O_k	Observability matrix
p	Pitch bearing position
$Q_{i\,k}$, $R_{ij\,k}$	QR factorization matrices of $U_{k,s}$ and $Y_{k,s}$, $(i,j) = \{1,2\}$
R	Blade radius
$U_{k,s}$, $Y_{k,s}$	Input and output Hankel matrices
U_k, Σ_k, V_k	Singular value decomposition matrices of $R_{22\,k}$
T_Z	Rotor thrust
u	System control
V	Electric potential
V_∞	Free stream velocity
w	White noise
W_{dist}	Baseline loads shaping filters
W_n	Disturbance shaping filters
W_{perf}	Performance weighting function
x, y	System state and output vectors
z	System performance
α	Shaft angle
ϑ_p	Precone angle
ϑ_{tw}	Blade twist
μ	Advancing ratio
ν_β	Non-dimensional flap frequency
ν_ϑ	Non-dimensional torsional frequency
ν_ξ	Non-dimensional lag frequency
Ω	Rotor angular velocity

1.0 INTRODUCTION

Helicopters experience severe levels of vibration on the main rotor due to the asymmetrical airflow in forward flight. These vibratory loads are transmitted to the fuselage and degrade the flight comfort, while causing structural components fatigue and wear. Active controls are being extensively investigated by helicopter researchers to reduce the related vibrations. The basic strategy to alleviate such loads is to modify the periodic aerodynamic loads at harmonic frequencies above the $1/rev$. The simplest approach is to control the already available swashplate through a suitable harmonic signal computed by the higher harmonic control (HHC) algorithm[1], based on a linear quasi-static rotor model response. However, it is now possible to embed actuators into the blades and thus to independently control each blade . This allows to overcome the limitations of using only swashplate as actuator, such as the need to install otherwise over-dimensioned hydraulic actuators and the impossibility to independently control more that three blades. Different methods of actuation have been studied to carry out individual blade control (IBC)[2,3,4,5]. In this paper we assume the availability of actively twisted blades. Piezoelectric actuators are distributed along the blade span, with the control voltage computed to minimize the aerodynamic loads. This

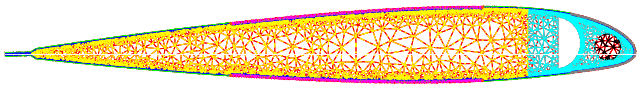

Figure 2.1: Blade section discretization.

solution has been widely investigated in recent years[6,7], and experimental tests carried out at NASA[2] and DLR[8,9] proved its feasibility.

The complex nonlinear behavior of the rotor subsystem in forward flight, limits the possibility of achieving satisfactory performance through linearized time invariant controller theories. In particular, the dynamic system periodicity plays an important role, so that more sophisticated solutions can be found by exploiting the periodic control theory. A model following approach to stabilize lag and pitch moments using periodic control has been proposed by Vaghi[10]. Periodic vibration controllers were also used by Arcara et al.[11] and by Bittanti and Cuzzola[12]; both these papers consider the baseline loads alleviation by means of IBC as a disturbance rejection problem. Active twist flaps are used by Ulker[13] to reduce hub loads by a dynamic compensator arising from the periodic H_2 and H_∞ design.

In the present paper we start from a review of the periodic H_2 design and of the periodic output feedback (POF) technique[14,15] to reduce hub loads. After comparing the two solutions and showing that satisfactory results can be achieved by using the static POF approach, we test the robustness of the two controllers. It is shown that, even if a simple design model is used in the design phase of the vibration periodic controllers, satisfactory loads reduction are achieved with a more complex numerical model that better approximates the real rotor behavior. An important aspect of this study is the analysis of the POF controller: its design is very simple and involves fewer parameters than those of the H_2 controller. It also allows to easily cover the whole helicopter flight envelope by an easier scheduling.

The paper is organized as follows. In the first part the rotor numerical model and the tools used to simulate the response of both the design and the validation model are described. In the second part the blade response of the design model is properly identified and the procedures to synthesize the periodic H_2 controller and the POF one are explained. The third and final part of the work shows the validation model closed loop results and assesses the controllers robustness.

2.0 NUMERICAL MODELING

2.1 Multibody rotor model

Vibratory forces acting on the hub can be reduced by modifying the periodic aerodynamic loads in forward flight condition. Blades actively twisted by means of piezoelectric actuators distributed along the blade span are considered here. The original blades of an already available multibody model of the Bo105 rotor[16] are replaced with actively twisted ones. The active blades use macro-fiber composite (MFC) piezoelectric actuators with interdigitated electrodes. These actuators exploit the primary piezoelectric direction of polarization, thus allowing to achieve a high strain rate with low actuation power. They are oriented in such a way that the strain is applied at ± 45 to generate maximum torsional authority.

The inertial couplings and structural deformation of the main helicopter rotor are intrinsically nonlinear. Therefore, the use of a suitable nonlinear model is mandatory. A deformable multibody model, built with the software MBDyn[17], is used. The swashplate and the pitch links are represented with rigid bodies, while each blade is modeled using five geometrically exact finite volume nonlinear beam elements[18]. MBDyn is able to handle piezoelectrically actuated beams provided the stiffness and the piezoelectric coupling matrices of the blade section are known. The beam section stiffness and mass data of the original Bo105 blades are known. The section properties of the actively twisted blades, on the contrary, have to be computed. An accurate way to compute such properties, still accounting for three dimensional elastic and piezoelectric constitutive laws, is the semi-analytical approach[19,20,21]. The three dimensional continuum is decomposed into the one dimensional domain of the beam model and the two dimensional domain of the beam section. A finite element discretization of the beam section, such as that shown in Fig. 2.1, allows to compute, by means of a specialized semi-analytic procedure, the sought generalized beam section stiffness matrix. This semi-analytical formulation was used to optimize the piezoelectric blade section[22]; the position of the elastic axis and of the center of mass were constrained during the optimization to avoid aeroelastic instabilities. Rotor data, together with the first frequencies of the original passive blades and of the optimized piezoelectric blades, are shown in Table 1.

Even if MBDyn is a general purpose multibody software, it contains some specialized elements for the simulation of helicopter rotors; among them, it provides simple aerodynamic elements, such as the blade element momentum theory and different linear inflow models. Taken together, these elements allow to quickly approximate the system response with a level

Table 1: **BO 105 model data with original and piezoelectric blade.**

Rotor data	**BO 105 blade**	**Piezoelectric blade**
R	4.9 m	4.9 m
p	0.23 m	0.23 m
ϑ_p	2.5°	2.5°
c	0.3025 m	0.3025 m
ϑ_{tw}	−8°	−8°
Ω	44.4 rad/s	44.4 rad/s
α	3°	3°
ν_β	1.11	1.1
ν_ξ	0.69	0.73
ν_ϑ	3.63	3.89

of accuracy that is deemed suitable to reproduce representative vibratory loads in forward flight, at least for a preliminary design of the controller. The simulations were performed by combining the blade element momentum (BEM) theory with the Drees inflow model[23]. The required data are the lift, drag and moment coefficients of the blade NACA 23012 airfoil, C_L, C_D and C_M, with respect to the Mach number and to the aerodynamic angle of attach. This rotor model will be later referred to as the "low fidelity model" because it is based on a low fidelity aerodynamic model. It has been used to design the controllers through several optimizations.

2.2 Free wake aerodynamic code

A more accurate model is required to validate the controllers performance. The multibody deformable structural model is detailed, well tested, and validated. The aerodynamic model, on the other hand, is rather simple, and can strongly influence the predicted loads acting on the blades. In particular, linear inflow models are known to underestimate the harmonic content of the forces. Computational fluid dynamics (CFD) is usually used to solve the aerodynamic field of every single blade, while the induced velocity is computed through potential methods, such as the prescribed or free wake method[24]. However, we strive to avoid computationally-intense tasks, such those arising from CFD simulations, because we need to simulate several seconds of flight to validate the controllers. For this reason we've chosen the so-called hybrid approach[25,26,27], thus treating separately, with different models, the aerodynamic near and far fields of the blade. An improved blade element theory accounting for unsteady effects is used for the near field representation. The rotor wake is approximated by releasing the blade tip vortex at each time step; the ensuing free wake dynamic is integrated in time, with the induced velocity computed according to the Biot-Savart law.

The blade span is divided into strips, with more elements at the blade root and tip; a tip loss factor is defined as well. The tip loss correction factor F scales the aerodynamic coefficients of each strip and is computed according to the simplified Prandtl's formulation[23,28]. The lift, drag and aerodynamic moment of the strip is computed through the data sheet for the C_L, C_D and C_M coefficients that was used for the MBDyn simulations and scaled by the tip loss factor F. The effective aerodynamic angle of attack, however, is corrected by accounting for unsteady effects; this is achieved by using both the Theodorsen lift deficiency function for the airfoil motion and the Kussner function, that better represents the interaction between the blades and the tip vortexes, considered as gusts[29,30].

After computing the loads of every blade element, the equivalent bound circulation is computed through the Kutta-Jukovsky theorem and the strength of the tip vortex that is going to be released at a given time step is set to the 80% of the maximum bound circulation of the blade outer portion[31], with a dual-peak model in case of a negative load on the outer portion of the blade tip[32]. An important model parameter is the size of the vortex core. Since we are only using the tip vortex to approximate the rotor wake, reproducing the physical size of the core vortex would overestimate the blade vortex interaction loads[27]; thus, we assume that the blade tip vortex initial diameter is equal to 50% of the blade chord[33], and that the vortex aging follows Squire's law[34,27]. The effects of the near wake are taken into account by the unsteady blade element theory and the tip loss correction; for this reason the far wake represented by the tip vortexes is activated after 30° of rotor revolution. The aerodynamic code is written in Matlab.

MBDyn can perform co-simulations by exchanging data with external programs by means of bidirectional socket communications; a Python communication library is available to ease the interfacing effort. Therefore, the Matlab free wake code is connected to MBDyn through the open-source software MatPy[35], a useful Python interpreter for Matlab. The

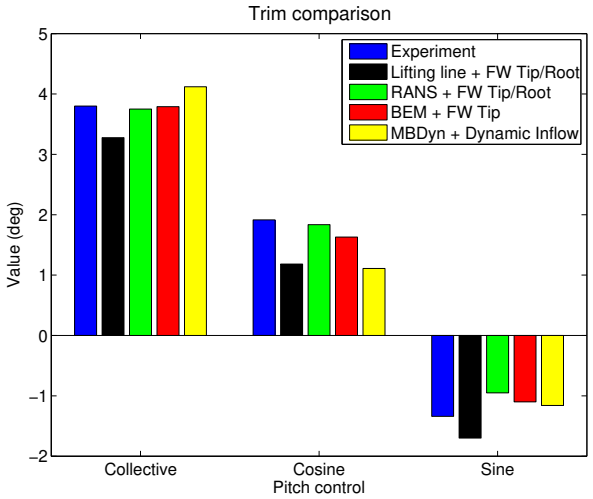

Figure 2.2: Hart II baseline trim condition, 6° descent flight at $\mu = 0.15$.

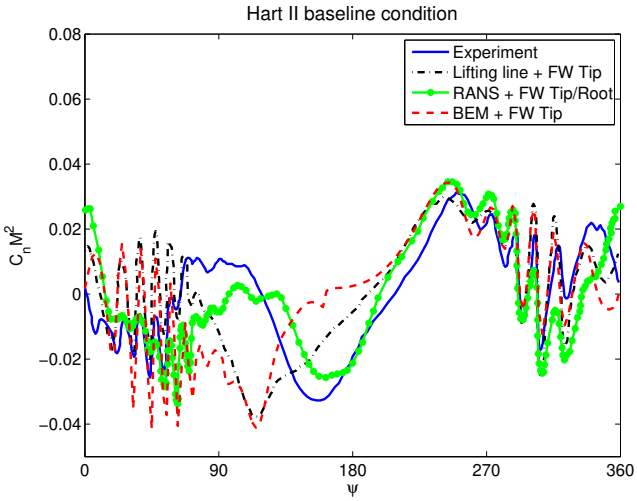

Figure 2.3: Normal force coefficient comparison, 87%R.

aeroelastic interface between the structural node of the beams and the aerodynamic strip elements is computed through an energy-conserving moving least squared algorithm[36].

The simulation code has been validated with the experimental data of the Hart II baseline trim condition, a 6° descent flight at $\mu = 0.15$[37]. Figure 2.2 compares the experimental collective and cyclic pitch control against those computed with our free wake code, with the blade element theory combined with the dynamic inflow of MBDyn, and with the two hybrid approaches described by Amiraux[38]. In the first approach the lifting line theory is combined with the free wake geometries of the tip and the root vortexes, while in the second approach a more accurate RANS-based CFD code is used for the near field aerodynamics of the blade. To better evaluate the BVI prediction and the loads estimation capabilities of the code, the normal force coefficient of the section at 87%R is compared, for one rotor revolution, in Fig. 2.3. The normal force coefficient predicted by our code is close to that obtained with the lifting line theory with only the free wake of tip vortex; it is also able to predict the position of the BVI. However, both codes overestimate the BVI peaks. The more accurate and computationally demanding RANS model with tip and root vortexes reduces the BVI peaks and better approximates the low frequency content of the normal force coefficient. Moreover, the lifting line and BEM methods produce a lower peak in C_nM^2 near 115 deg., while experiment and RANS solver lower peaks are closer to 160 deg. This phase shift will have an impact on $4/rev$ loads. Thus, the proposed code is not able to match the more accurate response of the RANS plus tip/root vortexes schemes. However, it reproduces with a much smaller computational cost the overall response of the real system. It will thus be used as a verification model to asses the proposed controller robustness.

3.0 CONTROLLER DESIGN

3.1 Identification of the design model

The design model, based on the low fidelity aerodynamic theory provided by MBDyn, allows to tune the controller with a reasonable computational effort. The effect of the control applied to one blade on the forces on the other blades is almost null due to the very simple aerodynamic model. Therefore, each blade is considered independent and the IBC controller is designed by considering only a single blade. A periodic state space model linearized around an equilibrium configuration is required for the periodic control design. The linearized input/output relation between the voltage V applied on the blade and the blade sensors measures is of interest. The blade root shear force F_z and five vertical accelerations at locations uniformly distributed along the blade span are chosen as outputs in order to well represent the blade response for the identification.

Dealing with a helicopter in forward flight, the system is periodic. This has to be taken into account while identifying the model. Classical identification procedures for linear time invariant (LTI) systems cannot be used for periodic systems. Thus, a periodic subspace identification algorithm[13] is used to find a linear discrete-time periodic (LTP) model of the blade in the form

$$\begin{aligned} \mathbf{x}_{k+1} &= \mathbf{A}_k \mathbf{x}_k + \mathbf{B}_k u_k, \\ \mathbf{y}_k &= \mathbf{C}_k \mathbf{x}_k, \end{aligned} \tag{3.1}$$

where the system matrices have period N. The input/output time histories signals from the numerical simulations are organized in input/output Hankel matrices $\mathbf{U}_{k,s}$ and $\mathbf{Y}_{k,s}$ for $k = 1...N$ as follows

$$\mathbf{U}_{k,s} = \begin{bmatrix} u_k & u_{k+1} & \cdots & u_{k+s-1} \\ u_{N+k} & u_{N+k+1} & \cdots & \vdots \\ \vdots & & \cdots & \vdots \\ u_{(n-1)N+k} & & \cdots & u_{(n-1)N+k+s-1} \end{bmatrix}, \tag{3.2}$$

$$\mathbf{Y}_{k,s} = \begin{bmatrix} y_k & y_{k+1} & \cdots & y_{k+s-1} \\ y_{N+k} & y_{N+k+1} & \cdots & \vdots \\ \vdots & & \cdots & \vdots \\ y_{(n-1)N+k} & & \cdots & y_{(n-1)N+k+s-1} \end{bmatrix}, \tag{3.3}$$

where N is the period, n is the total number of simulations and s is the length of each experiment. The Hankel matrices are computed using data from the numerical simulations. Considering the QR factorization of the compound matrices

$$\begin{bmatrix} \mathbf{U}_{k,s} & \mathbf{Y}_{k,s} \end{bmatrix} = \begin{bmatrix} \mathbf{Q}_{1_k} & \mathbf{Q}_{2_k} \end{bmatrix} \begin{bmatrix} \mathbf{R}_{11_k} & \mathbf{R}_{12_k} \\ \mathbf{R}_{21_k} & \mathbf{R}_{22_k} \end{bmatrix}, \tag{3.4}$$

the observability matrix $\mathbf{O}_k$ is given by the row space of matrix $\mathbf{R}_{22_k}$. It can be computed through the singular value decomposition (SVD)

$$\mathbf{R}_{22_k} = \mathbf{U}_k \Sigma_k \mathbf{V}_k^T \tag{3.5}$$

$$\mathbf{O}_k = \tilde{\mathbf{V}}_k^T. \tag{3.6}$$

The order of the identified system is chosen according to the magnitude of the singular values of Σ_k. Then, the observability matrix is computed as $\tilde{\mathbf{V}}_k^T$, which contains the first rows and columns of $\mathbf{V}_k^T$ up to the defined system order. Afterward, the matrices $\mathbf{A}_k$ and $\mathbf{C}_k$ can be obtained by exploiting the observability matrix at the instants $k+1$ and k[39,13]. The system periodicity is imposed by setting $\mathbf{O}_{N+1} = \mathbf{O}_1$.

Matrices $\mathbf{B}_k$ and $\mathbf{D}_k$ are computed by minimizing the squared 2-norm error between the real and the model outputs, y_{real} and y respectively:

$$\min_{\mathbf{B}_k, \mathbf{D}_k} \| y_{real} - y \|_2^2 . \tag{3.7}$$

The rotor is trimmed at an advance ratio $\mu = 0.23$ so to reproduce reasonable hub forces, $T_Z = 20010$ N, $M_X = 746$ Nm and $M_Y = -85$ Nm, with a shaft angle of $\alpha = 3^\circ$ as in Fig. 3.1. The blade periodic loads and the accelerations for the reference trimmed configuration are saved; they are subsequently subtracted from the excited response signals to linearize the system

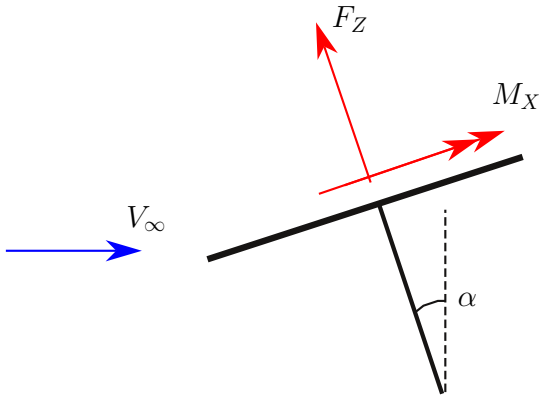

Figure 3.1: Rotor shaft inclination.

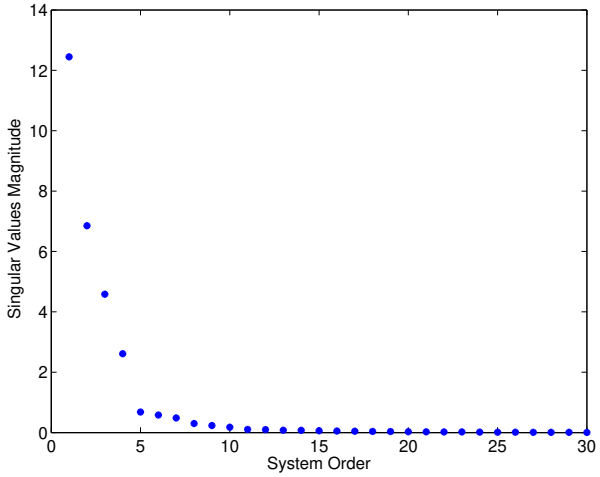

Figure 3.2: Hankel singular values magnitude of $\mathbf{R}_{22_k}$.

around the trimmed configuration. The blade are excited with a random voltage with an amplitude of 40 V filtered above $6/rev$ to limit higher harmonics in the dynamic response. Being the Bo105 a four blades rotor, the most important harmonics for the vibratory hub loads are the $3/rev$ and the $4/rev$; all output signals have been filtered before the identification to consider only these harmonics, hence reducing the size of the state space model. The controllers should minimize the $4/rev$ harmonic of the blade root shear force F_z to reduce the hub vertical force and reduce the $3/rev$ harmonic as well to alleviate the vibratory loads associated to the moments of the blade root loads. Note that for the vertical force and the torque of the hub only the steady and the multiples of the $4/rev$ harmonics of the blade root force and moment are not filtered by the hub. On the other hand, the multiples of the $4/rev$ in plane forces and moments of the hub, with respect to the rotor disk, are generated by the multiples of the $3/rev$ and $5/rev$ blade loads and moments. The aeroelastic multibody simulation requires a small integration time step; the simulations are performed with $N = 140$ time steps for every rotor revolution. The direct identification of such signals will lead to the computation of 140 linear systems spanning the period. The system outputs are decimated to $N = 28$ time steps per rotor revolution in order to reduce the computational burden of both the identification and the controller design, still approximating the outputs with sufficient accuracy. Hints about the order of the identified system can be found by analyzing the singular value magnitudes of the matrix $\mathbf{R}_{22_k}$ at each time step.The best compromise between data fitting and system order is given by retaining the most important singular values. For example, Fig. 3.2 shows the singular values computed for the first time step. Based on the singular values, the chosen linear periodic model of the blade is a $14th$ order system for every time step spanning the period.

After identifying the linearized blade model, performance specifications and model disturbances have to be introduced in

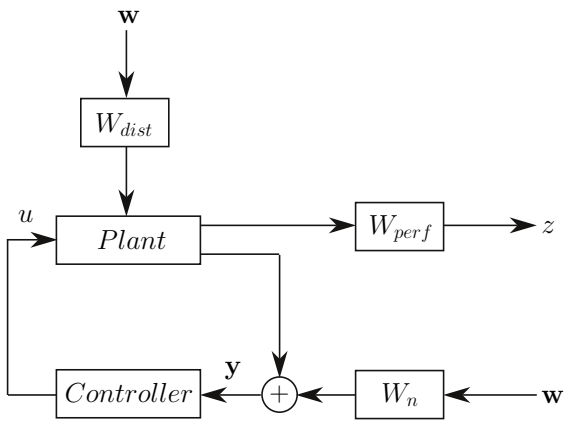

Figure 3.3: Generalized plant.

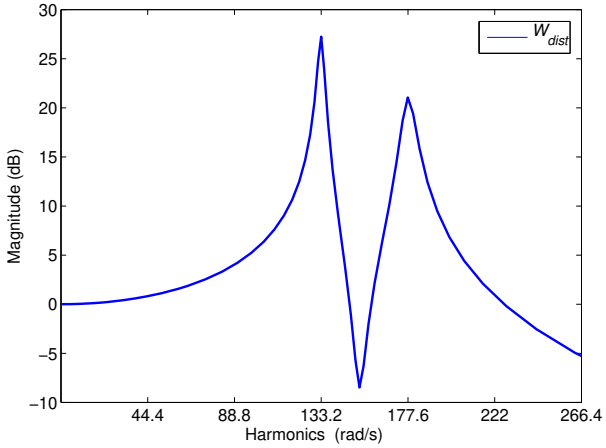

Figure 3.4: Shaping filter of the baseline tip vertical acceleration.

the generalized plant. The block diagram of the complete design model is shown in Fig. 3.3, where $\mathbf{z}$ are the controlled outputs, $\mathbf{y}$ are the measures, $\mathbf{w}$ are white noise disturbances and u the applied blade voltage. The goal is to minimize the blade root shear force F_z. The shaping filters W_{dist} models the baseline loads, which are now reintroduced as output disturbances of the system. Figure 3.4 shows the shaping filter that models the baseline load of the tip blade acceleration; since the measures have been previously filtered, only the $3/rev$ and the $4/rev$ harmonics of the baseline signals have to be reproduced. The sensors noise is modeled with white noises having an amplitude of 0.1. The performance of the controller are defined by means of the frequency weighting function W_{perf}, shown in the block diagram of Fig. 3.3, to impose the reduction of the blade root load F_z harmonics; it is adjusted in the controller design phase to obtain the best vibration reduction. The generalized plant model is thus described with the following linear periodic model

$$\begin{aligned} \mathbf{x}_{k+1} &= \mathbf{A}_k\mathbf{x}_k + \mathbf{B}_{1_k}\mathbf{w}_k + \mathbf{B}_{2_k}V_k, \\ \mathbf{z}_k &= \mathbf{C}_{1_k}\mathbf{x}_k + \mathbf{D}_{11_k}\mathbf{w}_k + \mathbf{D}_{12_k}V_k, \\ \mathbf{y}_k &= \mathbf{C}_{2_k}\mathbf{x}_k + \mathbf{D}_{21_k}\mathbf{w}_k. \end{aligned} \tag{3.8}$$

It can be noticed that there is no direct feedthrough between the input voltage and the sensor measures, i.e. matrix $\mathbf{D}_{22} = \mathbf{0}$.

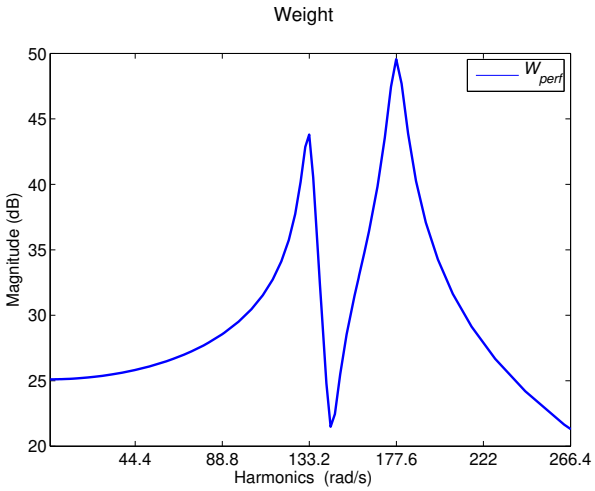

Figure 3.5: H_2 Control performance weight.

3.2 H_2 Periodic controller

This section describes the design of the optimal H_2 controller that stabilizes the system and minimizes the H_2 norm of the transfer function between the plant disturbance and the desired performance. Starting from the identified generalized plant model a dynamic output feedback controller can be found by solving two Discrete Time Periodic Riccati Equations (DTPRE)[40] corresponding to the filtering and the state feedback control problem:

$$\begin{aligned}\mathbf{Q}_{k+1} &= \mathbf{A}_k\mathbf{Q}_k A_k^T + \mathbf{B}_{1_k}\mathbf{B}_{1k}^T - \left(\mathbf{A}_k\mathbf{Q}_k\mathbf{C}_{2_k}^T + \mathbf{B}_{1_k}\mathbf{D}_{21_k}^T\right) \\ &+ \left(\mathbf{D}_{21_k}\mathbf{D}_{21_k}^T + \mathbf{C}_{2_k}\mathbf{Q}_k\mathbf{C}_{2_k}^T\right)^{-1}\left(\mathbf{A}_k\mathbf{Q}_k\mathbf{C}_{2_k}^T + \mathbf{B}_{1_k}\mathbf{D}_{21_k}^T\right),\end{aligned} \tag{3.9}$$

$$\begin{aligned}\mathbf{P}_k &= \mathbf{A}_k^T\mathbf{P}_{k+1}\mathbf{A}_k + \mathbf{C}_{1_k}^T\mathbf{C}_{1_k} - \left(\mathbf{A}_k^T\mathbf{P}_{k+1}\mathbf{B}_{2_k} + \mathbf{C}_{1_k}^T\mathbf{D}_{12_k}\right) \\ &+ \left(\mathbf{D}_{12_k}^T\mathbf{D}_{12_k} + \mathbf{B}_{2_k}^T\mathbf{P}_{k+1}\mathbf{B}_{2_k}\right)^{-1}\left(\mathbf{A}_k^T\mathbf{P}_{k+1}\mathbf{B}_{2_k} + \mathbf{C}_{1_k}^T\mathbf{D}_{12_k}\right).\end{aligned} \tag{3.10}$$

A cyclic QZ decomposition method is used for the solution of eqs. 3.9 and 3.10[41,42]. Once the solutions of the Riccati equations have been obtained, the periodic control system can be easily defined by[40,13]

$$\begin{aligned}\xi_{k+1} &= \mathbf{A}_k^C\xi_k + \mathbf{B}_k^C\mathbf{y}_k, \\ V_k &= \mathbf{C}_k^C\xi_k + \mathbf{D}_k^C\mathbf{y}_k.\end{aligned} \tag{3.11}$$

The controller matrices $\mathbf{A}_k^C$, $\mathbf{B}_k^C$, $\mathbf{C}_k^C$ and $\mathbf{D}_k^C$ can be computed by following the procedure shown in the Appendix[14].

The controller has the same order of the generalized plant of eq. 3.8, and depends on the selected frequency weighting functions and shaping filters for performance specification and the disturbance modeling. A good compromise between control activity and loads alleviation is found by using the performance frequency weighting function W_{perf} shown in Fig. 3.5. The resulting periodic controller is a $44th$ order dynamic compensator with period $N = 28$. The controller is designed for the first blade; the same controller is used for the other blades after applying a time shift to its matrices to account for the system periodicity.

3.3 Periodic output feedback controller

The second approach analyzed in this paper is a periodic static controller. The control law is a direct feedback relationship of the form

$$\mathbf{u}_k = \mathbf{K}_k\mathbf{y}_k,$$

where the gain matrix $\mathbf{K}_k$ can either be periodic with period N or a constant matrix equal for all sample times. The static output feedback control law is obtained by minimizing the quadratic performance index

$$J = E\left[\sum_{k=0}^{\infty}\left(\mathbf{z}_k^T\mathbf{Q}_k\mathbf{z}_k + \mathbf{u}_k^T\mathbf{R}_k\mathbf{u}_k\right)\right], \tag{3.12}$$

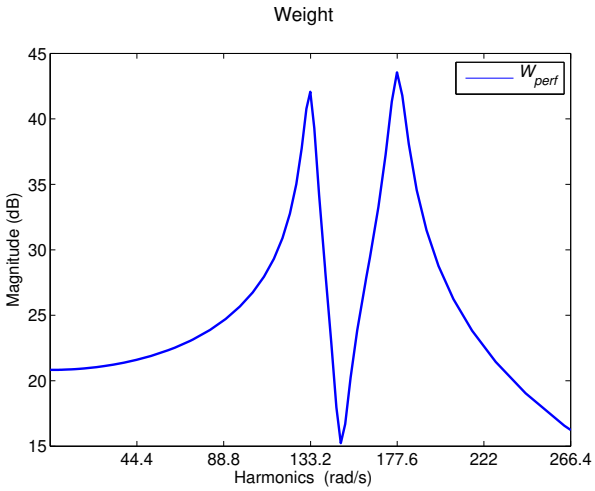

Figure 3.6: POF Control performance weight.

where $\mathbf{Q}_k$ and $\mathbf{R}_k$ are symmetric periodic user defined weighting matrices. No closed form solutions can be found to this problem. Its solution must be found by resorting to a numerical optimization procedure. The problem can be reformulated as[43]

$$J(\mathscr{K}) = tr(\sigma\mathscr{P}\mathscr{G}), \tag{3.13}$$

$$\nabla_{\mathscr{K}} J(\mathscr{K}) = 2(\mathscr{R}\mathscr{K}\mathscr{C}_2 + \mathscr{B}_2^T \sigma\mathscr{P}\overline{\mathscr{A}})\mathscr{S}\mathscr{C}_2^T, \tag{3.14}$$

where the gradient of the cost function is provided as well, since many optimization algorithms require it. The script notation $\mathscr{X}$ indicates the block diagonal matrix $\mathscr{X} = diag(\mathbf{X}_1, \ldots, \mathbf{X}_N)$ related to the cyclic sequence of the periodic matrix $\mathbf{X}_k$; the notation $\sigma\mathscr{X}$ denotes the K-cyclic shift $\sigma\mathscr{X} = diag(\mathbf{X}_2, \ldots, \mathbf{X}_N, \mathbf{X}_1)$. Matrices $\mathscr{P}$ and $\mathscr{S}$ satisfy the Discrete Periodic Lyapunov Equations (DPLEs)

$$\mathscr{P} = \overline{\mathscr{A}}^T \sigma\mathscr{P}\overline{\mathscr{A}} + \overline{\mathscr{Q}} \tag{3.15}$$

and

$$\sigma\mathscr{S} = \overline{\mathscr{A}}\mathscr{S}\overline{\mathscr{A}}^T + \mathscr{G} \tag{3.16}$$

respectively, where $\overline{\mathscr{A}} = \mathscr{A} + \mathscr{B}_2\mathscr{K}\mathscr{C}_2$ is the closed loop matrix and $\overline{\mathscr{Q}} = \mathscr{Q} + \mathscr{C}_2^T\mathscr{K}^T\mathscr{R}\mathscr{K}\mathscr{C}_2$. Algorithms for the solution of DPLEs are described by Varga[44] and Varga and Pieters[43]. Matrix $\mathscr{G}$ is defined as $\mathscr{G} = diag(0, \ldots, 0, \mathbf{X}_0)$, where $\mathbf{X}_0$ represents the influence of initial conditions and disturbances on the state dynamics defined as $\mathbf{X}_0 = E\left[\bar{\mathbf{x}}_0\bar{\mathbf{x}}_0^T\right]$. In the closed loop system the perturbed initial conditions are

$$\bar{\mathbf{x}}_0 = \mathbf{x}_0 + (\mathbf{B}_{1_N} + \mathbf{B}_{2_N}\mathbf{K}_N\mathbf{D}_{21_N})\,\mathbf{w}. \tag{3.17}$$

Assuming null cross-correlation between the initial conditions $\mathbf{x}_0$ and the disturbances $\mathbf{w}$, i.e. $E\left[\mathbf{x}_0\mathbf{w}^T\right] = 0$, the matrix $\mathbf{X}_0$ is given by

$$\begin{aligned}\mathbf{X}_0 \;=\; & E\left[\mathbf{x}_0\mathbf{x}_0^T\right] + \mathbf{B}_{1_N}E\left[\mathbf{w}\mathbf{w}^T\right]\mathbf{B}_{1_N}^T + \mathbf{B}_{2_N}\mathbf{K}_N\mathbf{D}_{21_N}E\left[\mathbf{w}\mathbf{w}^T\right]\mathbf{B}_{1_N}^T + \\ & \mathbf{B}_{1_N}E\left[\mathbf{w}\mathbf{w}^T\right]\mathbf{D}_{21_N}^T\mathbf{K}_N^T\mathbf{B}_{2_N}^T + \mathbf{B}_{2_N}\mathbf{K}_N\mathbf{D}_{21_N}E\left[\mathbf{w}\mathbf{w}^T\right]\mathbf{D}_{21_N}^T\mathbf{K}_N^T\mathbf{B}_{2_N}^T,\end{aligned} \tag{3.18}$$

where the variance matrices are approximated as identity matrices.

A constant (1×6) static gain matrix $\mathbf{K}$ is chosen for the control law. Since the dynamic model of the blade is already stable, the initial solution for the optimization procedure can be assumed as the null matrix. The performance specification has been adapted to achieve satisfactory results, resulting in a decrease of the weight effect on the $4/rev$ harmonic; the hand-tuned frequency weighting function W_{perf}, shown in Fig. 3.6, is similar to the H_2 controller weighting function of Fig. 3.5. The performance weighting matrix $\mathbf{Q}_k$ of the cost function J is the identity matrix, because the performance specifications have been taken into account by W_{perf}, and is kept constant for the whole period. The weight matrix $\mathbf{R}_k$, that prescribes further limitation for the control signal, is tuned until satisfactory loads reduction is achieved. In this example it has a value of $5{,}000$. The design of this controller is faster than that of the H_2 one because of the smaller number of parameters involved in the optimization and because the solution of the two DPLEs is less demanding than the solution of the DTPREs[42].

4.0 SIMULATION RESULTS

4.1 Closed loop analysis on the design model

The performance of the periodic controllers, designed on the multibody rotor model with low fidelity aerodynamics, are shown at $\mu = 0.23$. The periodic controllers are implemented in Simulink environment using S-functions. Rate-transition blocks are used before and after the controller because of the different sample times between the multibody simulation and the periodic controller.

The vibration reduction achieved by the periodic controllers are summarized in Fig. 4.1. Although a significant passive load reduction is obtained by simply replacing the Bo105 blades with the piezoelectric ones, both controllers allow to further alleviate the hub loads. The H_2 controller reduces the $4/rev$ harmonic of the hub force and moments F_Z, M_X and M_Y by 24%, 60% and 86%, respectively. The static output feedback controller achieve a reduction of 43%, 65% and 58%. Both solutions are satisfactory, and their performances are comparable. The H_2 controller has a better capability to reduce the moment M_Y, while the direct output feedback approach better alleviates F_Z. On the average, the simpler static output feedback controller can be a valid substitute of the H_2 controller dynamic compensator, in spite of its faster algorithm and fewer design parameters. Note also that harmonics higher than the $4/rev$ are only marginally excited.

The voltage applied on the first blade is shown in Fig. 4.2. The control signal is a sequence of steps because of the controller sampling time. The control effort remains quite low, and doesn't exceed 80 V in both simulations. Note also that the control voltage computed by the static output feedback control has a lower frequency content than that of the H_2 dynamic compensator; this may lead to better robustness properties, since it doesn't excite high frequency harmonics that may not have been considered in the controller design phase.

4.2 Controller robustness validation

In this section the periodic controllers designed using the simple aerodynamic model are tested with the model coupled with the free-wake code. Figure 4.3 shows the computed rotor wake and the nondimensional inflow for the baseline condition. Dealing with the time marching wake of the tip vortexes, it is possible to model the blade vortex interaction and to have a good approximation of the induced velocity of the rotor. This validation model is a useful test-bed for robustness validation because the dynamics of the blades is different, since the swashplate setting is changed to reach the same trim configuration of the previous model. Furthermore, the induced velocity, that is better approximated, increases the harmonic content of the aerodynamic loads. In fact, the baseline loads of Fig. 4.4, estimated with the free wake model, are one order of magnitude higher than those those of Fig. 4.1, that were estimated with the simple inflow model.

Even if the improved aerodynamic model introduces new dynamics and raises the hub loads, none of the two controllers destabilize the rotor system, and they both achieve a good reduction of the loads. Both controllers reduce by more than 75% the moment M_X of Fig. 4.4b. The static output feedback controller seems to be more robust with respect to the force F_Z of Fig. 4.4b, and allows a larger reduction than that of the H_2 controller. This behavior could be explained by the fact that the H_2 control leads to an augmented periodic state space dynamic system with many controller parameters to be designed and additional dynamics in the closed loop system. On the contrary, the direct output feedback control law is based on a simple gain matrix that is kept constant throughout the period of the system.

Figure 4.5 shows the applied control voltage. The control activity is significantly higher than that of Fig. 4.2 because of the higher loads; still, it remains bounded and acceptable, since it is not higher than 800 V. This somewhat high voltage for control purposes may be a problem for crew safety. It is however within the range of what can be found in the literature. For example, in [2] the active twist blades are excited with an amplitude of $1,000$ V to assess vibrations reduction capabilities, while in [45] a voltage of ± 500 V is applied for blade de-icing.

5.0 CONCLUSIONS

A multibody numerical model of the Bo105 main rotor is modified by adding actively twisted blades, and used to design and implement individual blade control for hub vibration reduction relying on the periodic control theory. After identifying a periodic linearized model of the blade response, both the dynamic compensator arising from the H_2 periodic control theory and the periodic static output feedback controller, which minimize the $3/rev$ and the $4/rev$ harmonics of the blade root shear force, have been designed and tested. The closed loop simulations are carried out by coupling MBDyn and Simulink. The controllers are validated on a more sophisticated free wake aerodynamic model.

The design model shows a significant vibratory loads reduction with a small control effort, especially for the two hub moments M_X and M_Y. Furthermore, the performance of the two periodic controller appears to be similar. This means that

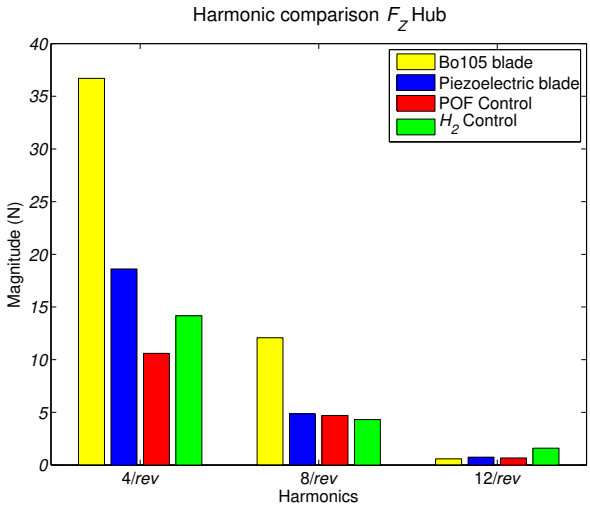

(a) Hub vertical force F_Z.

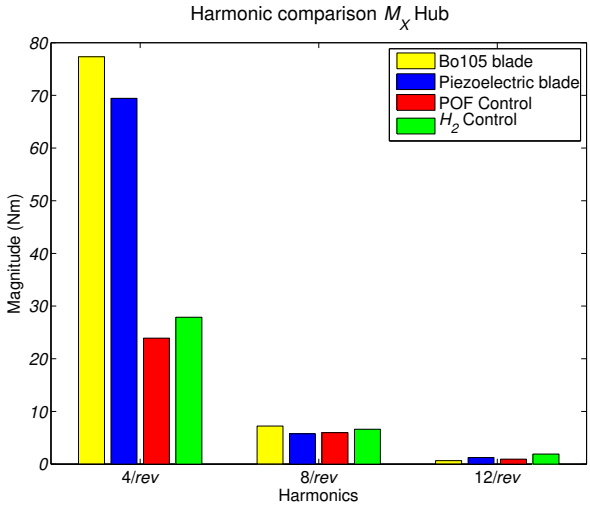

(b) Hub moment M_X.

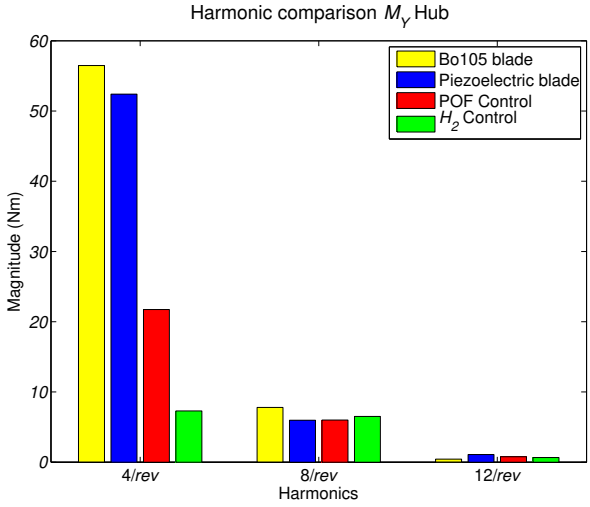

(c) Hub moment M_Y.

Figure 4.1: Vibrations reduction on the low fidelity model at $\mu = 0.23$.

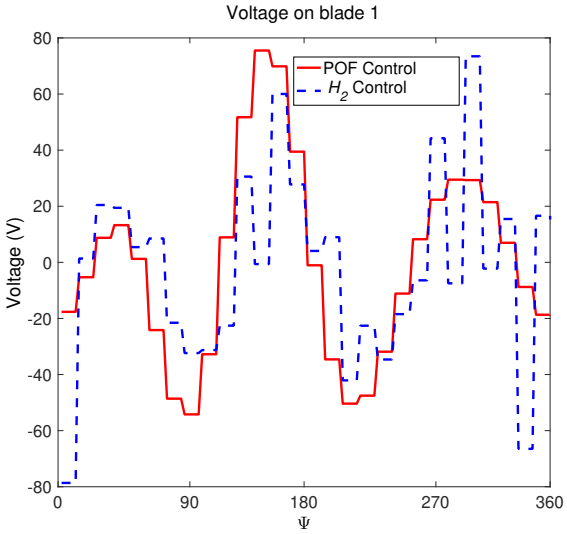

Figure 4.2: Applied voltage on blade 1 at $\mu = 0.23$, design model.

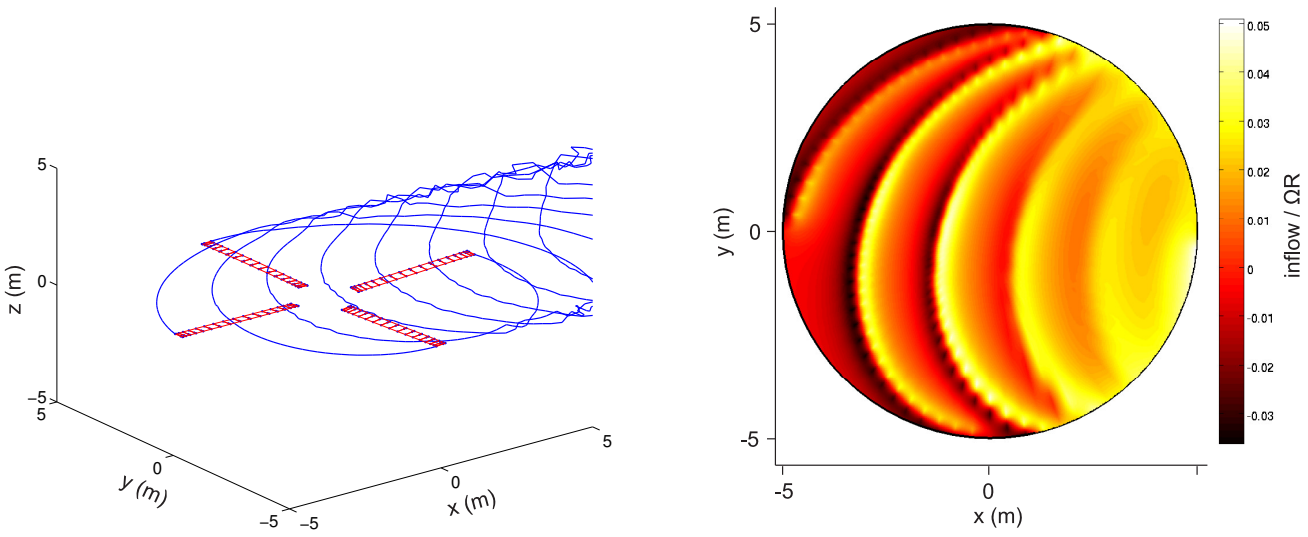

(a) Rotor wake.

(b) Non dimensional inflow at azimuth $\psi = 0°$.

Figure 4.3: Free wake aerodynamics (baseline condition at $\mu = 0.23$).

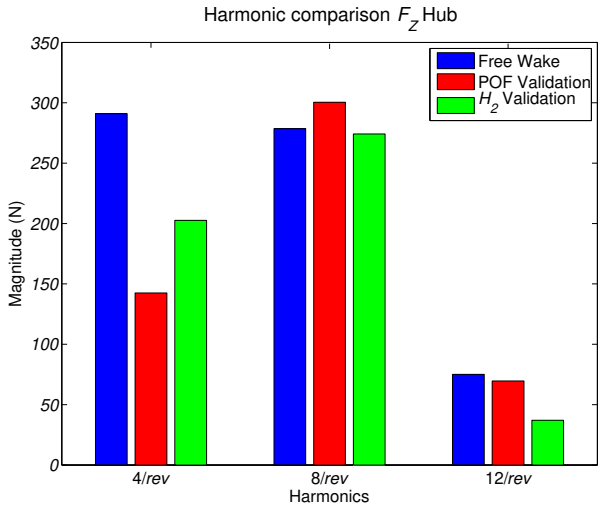

(a) Hub vertical force F_Z.

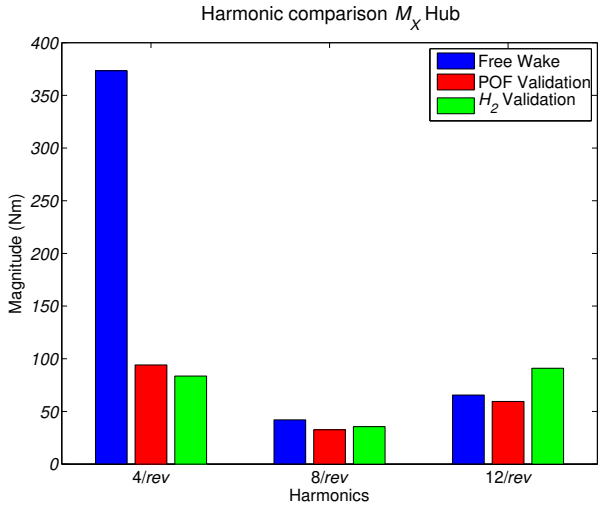

(b) Hub moment M_X.

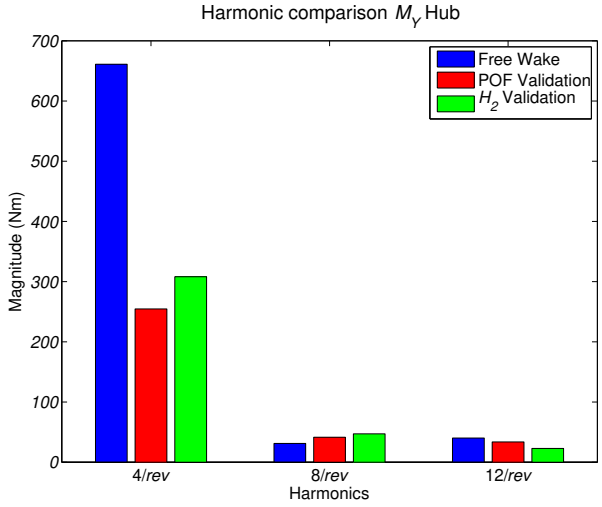

(c) Hub moment M_Y.

Figure 4.4: Validation of the controllers on the free wake model using the piezoelectric blade.

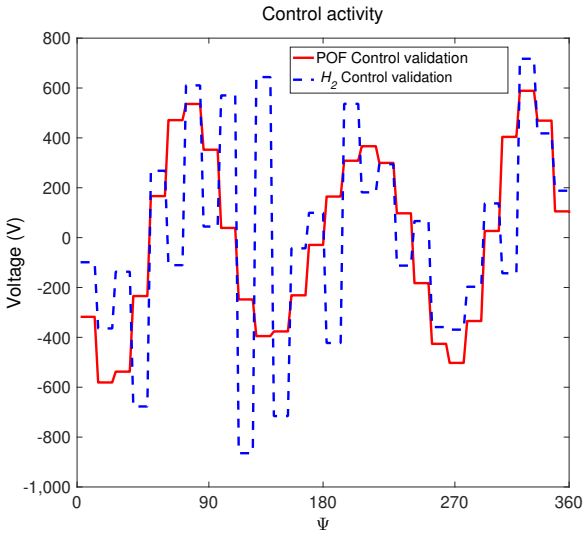

Figure 4.5: Applied voltage on blade 1 in the validation phase, $\mu = 0.23$, free wake.

the direct periodic output feedback, which involves fewer design parameters and has a faster design algorithm, can be a valid substitute of the optimal H_2 approach. Moreover, using only a gain matrix in the control law would allow to cover all the flight envelope by simply interpolating , with a gain scheduling technique, the gain matrices. It would thus be possible to avoid the problems that could arise when interpolating state space models [46,47].

The validation model, with the free wake aerodynamic code, shows that taking into account the periodicity of the rotor in forward flight leads to robust controllers even if model uncertainties are not considered in the design phase. In fact, there is no spillover, and both of the controllers manage to reduce vibratory loads with satisfactory performance. These results seems promising for a practical implementation of such controllers.

It must be noted, however, that the robustness of these periodic controllers still has to be thoroughly investigated for a large number of trim configurations. The effectiveness of the envisioned static output feedback gain scheduling has also to be assessed.

REFERENCES

1. PATT, D., CHANDRASEKAR, J., BERNSTEIN, D.S. and FRIEDMANN, P.P. Higher-harmonic-control algorithm for helicopter vibration reduction revisited. *Journal of Guidance, Control and Dynamics*, **28**, (5), September-October 2005.
2. WILBUR, M.L. and WILKIE, W.K. *Active-Twist Rotor Control Applications for UAVs*. Tech. rep., U.S. Army Research Laboratory Vehicle Technology Directorate, 2004.
3. MANDER, A., FESZTY, D. and NITZSCHE, F. Active pitch link actuator for impedance control of helicopter vibration. In *American Helicopter Society 64th Annual Forum*, April 29-May 1 2008.
4. PADTHE, A.K. and FRIEDMANN, P.P. Simultaneous BVI noise and vibration reduction in rotorcraft using microflaps including the effect of actuator saturation. In *American Helicopter Society 68th Annual Forum*, May 1-3 2012.
5. RAVICHANDRAN, K., CHOPRA, I., WAKE, B.E. and HEIN, B. Active pitch link actuator for impedance control of helicopter vibration. In *American Helicopter Society 67th Annual Forum*, 2011.
6. PAWAR, P.M. and JUNG, S.N. Active twist control methodology for vibration reduction of a helicopter with dissimilar rotor system. *Smart Materials and Structures*, **18**, (3), 2009, p. 035013. .
7. ALTHOFF, M., PATIL, M.J. and TRAUGOTT, J.P. Nonlinear modeling and control design of active helicopter blades. *Journal of the American Helicopter Society*, **57**, (1), 2012, pp 1–11(11). .
8. MONNER, H.P., RIEMENSCHNEIDER, J., OPITZ, S. and SCHULZ, M. Development of active twist rotors at the German Aerospace Center (DLR). In *52nd AIAA/ASME/ASCE/AHS/ASC Structures, Structural Dynamics and Materials Conference*. American Institute of Aeronautics and Astronautics, April 4-7 2011. AIAA 2011-1824.

9. RIEMENSCHNEIDER, J. and OPITZ, S. Measurement of twist deflection in active twist rotor. *Aerospace Science and Technology*, **15**, (3), 2011, pp 216–223. .
10. VAGHI, R. *Studio Numerico del Controllo Ottimo di un Rotore Articolato di Elicottero con Applicazione alle Instabilitá di Flappeggio e Ritardo*. Master Thesis, Politecnico di Milano, Dipartimento di Ingegneria Aerospaziale, 1991.
11. ARCARA, P., BITTANTI, S. and LOVERA, M. Periodic control of helicopter rotors for attenuation of vibrations in forward flight. *IEEE Transaction on Control Systems Technology*, **8**, (6), 2000, pp 883–894.
12. BITTANTI, S. and CUZZOLA, F.A. Periodic active control of vibrations in helicopters: a gain-scheduled multi-objective approach. *Control Engineering Practice*, **10**, (10), 2002, pp 1043–1057.
13. ULKER, F.D. *A New Framework For Helicopter Vibration Suppression; Time-Periodic System Identification and Controller Design*. PhD Thesis, Ottawa-Carleton Institute for Mechanical and Aerospace Engineering, April, 2011.
14. BRILLANTE, C., MORANDINI, M. and MANTEGAZZA, P. H2 periodic control on active twist rotor for vibration reduction. In *AHS 70th Annual Forum and Technology Display*, May 20-22 2014.
15. BRILLANTE, C., MORANDINI, M. and MANTEGAZZA, P. Periodic output feedback control for helicopter vibration reduction. In *International Forum on Aeroelasticity and Structural Dynamics*, June 28-July 2 2015.
16. DIETERICH, O., GÖTZ, J., DANGVU, B., HAVERDINGS, H., MASARATI, P., PAVEL, M., JUMP, M. and MASSIMILIANO, G. Adverse rotorcraft-pilot coupling: Recent research activities in Europe. In *34th European Rotorcraft Forum (ERF)*, September 16-19 2008.
17. MASARATI, P., MORANDINI, M. and MANTEGAZZA, P. An efficient formulation for general-purpose multibody/multiphysics analysis. *ASME J Comput Nonlinear Dyn*, 2013. .
18. GHIRINGHELLI, G.L., MASARATI, P. and MANTEGAZZA, P. Multibody implementation of finite volume C0 beams. *AIAA Journal*, **38**, (1), January 2000, pp 131–138.
19. GHIRINGHELLI, G.L., MASARATI, P. and MANTEGAZZA, P. Characterisation of anisotropic, non-homogeneous beam sections with embedded piezo-electric materials. *Journal of Intelligent Material Systems and Structures*, **8**, (10), October 1997, pp 842–858. .
20. MORANDINI, M., CHIERICHETTI, M. and MANTEGAZZA, P. Characteristic behavior of prismatic anisotropic beam via generalized eigenvectors. *International Journal of Solids and Structures*, **47**, (10), 2010, pp 1327–1337. .
21. BRILLANTE, C., MORANDINI, M. and MANTEGAZZA, P. Characterization of beam stiffness matrix with embedded piezoelectric devices via generalized eigenvectors. *International Journal of Solids and Structures*, **59**, 2015, pp 37–45. .
22. GHIRINGHELLI, G.L., MASARATI, P., MORANDINI, M. and MUFFO, D. Integrated aeroservoelastic analysis of induced strain rotor blades. *Mechanics of Advanced Materials and Structures*, **15**, 2008, pp 291–306. .
23. LEISHMAN, G.J. *Principles of Helicopter Aerodynamics*. Cambridge University Press, 2nd edn., Apr 2006. ISBN 978-0-521-85860-1.
24. ABEDI, H. *Development of Vortex Filament Method for Aerodynamic Loads on Rotor Blades*. Master's thesis, Chalmers University of Technology, Department of Applied Mechanics, Gothenburg, Sweden, 2013.
25. SHENG, C., ZHAO, Q., RAJMOHAN, N. and SANKAR, L. An unstructured hybrid CFD approach for computing rotor wake flows. In *49th AIAA Aerospace Sciences Meeting including the New Horizons Forum and Aerospace Exposition, Orlando, Florida*, Jan 4-7 2011.
26. YONGJIE, S., QIJUN, Z., FENG, F. and GUOHUA, X. A new single-blade based hybrid CFD method for hovering and forward-flight rotor computation. *Chinese Journal of Aeronautics*, **24**, 2011, pp 127–135.
27. AMIRAUX, M. *Numerical Simulation and Validation of Helicopter Blade-Vortex Interaction Using Coupled Computational CFD/CSD and Three Levels of Aerodynamic Modeling*. Ph.D. thesis, University of Maryland, Department of Aerospace Engineering, 2014.
28. BETZ, A. Schraubenpropeller mit geringstem Energieverlust. Mit einem Zusatz von l. Prandtl. *Nachrichten von der Gesellschaft der Wissenschaften zu GÃ¶ttingen, Mathematisch-Physikalische Klasse*, 1919, pp 193–217. URL `https://eudml.org/doc/59049`.
29. BISPLINGHOFF, R.L., ASHLEY, H. and HALFMAN, R.L. *Aeroelasticity*. Dover Publications, 2013.
30. HANSEN, M.H., GAUNAA, M. and MADSEN, H.A. *A Beddoes-Leishman Type Dynamic Stall Model in State-Space and Indicial Formulations*. Tech. Rep. 1354, Riso National Laboratory, June 2004.
31. VERMEER, L.J. A review of wind turbine wake research at TUDelft. In *20th 2001 ASME Wind Energy Symposium,*

Aerospace Sciences Meetings, 2001. AIAA 2001-0030.

32. JOHNSON, W. Influence of wake models on calculated tiltrotor aerodynamics. In *American Helicopter Society Aerodynamics, Acoustics, and Test and Evaluation Technical Specialists Meeting*, January 23-25 2002.
33. JOHNSON, W. A general free wake geometry calculation for wings and rotors. In *American Helicopter Society 51st Annual Forum*, May 9-11 1995.
34. LEISHMAN, J.G., BHAGWAT, M.J. and ANANTHAN, S. Free-vortex wake predictions of the vortex ring state for single-rotor and multi-rotor configurations. In *58th Annual Forum and Technology Display of the American Helicopter Society International*, June 11-13 2002.
35. MatPy – call Python from MATLAB. `http://algoholic.eu/matpy/`.
36. QUARANTA, G., MASARATI, P. and MANTEGAZZA, P. A conservative mesh-free approach for fluid-structure interface problems. In *International Conference for Coupled Problems in Science and Engineering*, May 23-29 2005.
37. SA, J.H., KIM, J.W., PARK, S.H., YOU, Y.H., PARK, J.S., JUNG, S.N. and YU, Y.H. Prediction of HART II airloads considering fuselage effect and elastic blade deformation. In *Heli Japan*, November 1-3 2010.
38. AMIRAUX, M. *Numerical Simulation and Validation of Helicopter Blade-Vortex Interaction Using Coupled Computational CFD/CSD and Three Levels of Aerodynamic Modeling*. Ph.D. thesis, University of Maryland, Department of Aerospace Engineering, 2014.
39. VERHAEGEN, M. and YU, X. A class of subspace model identification algorithms to identify periodically and arbitrarily time-varying systems. *Automatica*, **31**, (2), 1995, pp 201–216.
40. BITTANTI, S. and COLANERI, P. *Periodic Systems Filtering and Control*. Springer, 2009.
41. HENCH, J.J. and LAUB, A.J. Numerical solution of the discrete-time periodic Riccati equation. *IEEE Transaction on Automatic Control*, **39**, (6), Jun 1994, pp 1197–1210.
42. VARGA, A. On solving periodic Riccati equations. *Numerical Linear Algebra with Applications*, **15**, (9), August 2008, pp 809–835. .
43. VARGA, A. and PIETERS, S. A computational approach for optimal periodic output feedback control. In *IEEE International Symposium on Computer Aided Control System Design - CACSD*, 1996, pp 176–181. .
44. VARGA, A. Periodic lyapounov equations: Some applications and new algorithms. *International Journal of Control*, **67**, 1997, pp 69–88.
45. SCHULZ, M. and RIEMENSCHNEIDER, J. Investigation of active twist rotor for blade de-icing. In *American Helicopter Society 69th Annual Forum*, May 21-23 2013.
46. AMSALLEM, D. *Interpolation on Manifolds of CFD-Based Fluid and Finite Element-Based Structural Reduced-Order Models for On-Line Aeroelastic Predictions*. Ph.D. thesis, Stanford University, Department of Aeronautics and Astronautics, 2010.
47. CAIGNY, J.D., CAMINO, J.F. and SWEVERS, J. Interpolation-based modeling of MIMO LPV systems. *IEEE Transactions on Control Systems Technology*, **19**, (1), 2011, pp 46–63. .
48. ZHOU, K. and DOYLE, J.C. *Essentials of Robust Control*. Prentice Hall, 1997.

Appendix

Controller Matrices Reconstruction

The controller matrices $\mathbf{A}_k^C$, $\mathbf{B}_k^C$, $\mathbf{C}_k^C$ and $\mathbf{D}_k^C$ of eqs. 3.11 can be computed by following the procedure outlined in[13] and reported here for completeness. It can be derived by the filtering and control theory in H_2 described in[40] by combining the observer and the full information state feedback control.

After solving the two periodic Riccati eqs. 3.9 and 3.10, the sought matrices are given by

$$\mathbf{A}_k^C = \mathbf{A}_k - \mathbf{L}_k\mathbf{C}_{2_k} + \mathbf{B}_{2_k}\mathbf{K}_k - \mathbf{B}_{2_k}\mathbf{L}_k^O\mathbf{C}_{2_k}, \tag{5.1}$$

$$\mathbf{B}_k^C = \mathbf{L}_k + \mathbf{B}_{2_k}\mathbf{L}_k^O, \tag{5.2}$$

$$\mathbf{C}_k^C = \mathbf{K}_k - \mathbf{L}_k^O\mathbf{C}_{2_k}, \tag{5.3}$$

$$\mathbf{D}_k^C = \mathbf{L}_k^O, \tag{5.4}$$

where

$$\mathbf{L}_k = \left(\mathbf{A}_k\mathbf{Q}_k\mathbf{C}_{2_k}^T + \mathbf{B}_{1_k}\mathbf{D}_{21_k}^T\right)\left(\mathbf{C}_{2_k}\mathbf{Q}_k\mathbf{C}_{2_k}^T + \mathbf{D}_{21_k}\mathbf{D}_{21_k}^T\right)^{-1}, \tag{5.5}$$

$$\mathbf{L}_k^O = \left(\mathbf{K}_k\mathbf{Q}_k\mathbf{C}_{2_k}^T + \mathbf{W}_k\mathbf{D}_{21_k}^T\right)\left(\mathbf{C}_{2_k}\mathbf{Q}_k\mathbf{C}_{2_k}^T + \mathbf{D}_{21_k}\mathbf{D}_{21_k}^T\right)^{-1}, \tag{5.6}$$

$$\mathbf{K}_k = -\left(\mathbf{B}_{2_k}^T\mathbf{P}_{k+1}\mathbf{B}_{2_k} + \mathbf{D}_{12_k}^T\mathbf{D}_{12_k}\right)^{-1}\left(\mathbf{B}_{2_k}^T\mathbf{P}_{k+1}\mathbf{A}_k + \mathbf{D}_{12_k}^T\mathbf{C}_{1_k}\right) \tag{5.7}$$

and

$$\mathbf{W}_k = -\left(\mathbf{B}_{2_k}^T\mathbf{P}_{k+1}\mathbf{B}_{2_k} + \mathbf{D}_{12_k}^T\mathbf{D}_{12_k}\right)^{-1}\left(\mathbf{B}_{2_k}^T\mathbf{P}_{k+1}\mathbf{B}_{1_k} + \mathbf{D}_{12_k}^T\mathbf{D}_{11_k}\right). \tag{5.8}$$

Should matrix $\mathbf{D}_{22_k}$ be non null, i.e. should direct feedthrough be present, then the matrices would have to be modified into[48]

$$\tilde{\mathbf{A}}_k^C = \mathbf{A}_k^C - \mathbf{B}_k^C\mathbf{D}_{22_k}\mathbf{T}_k^{-1}\mathbf{C}_k^C, \tag{5.9}$$

$$\tilde{\mathbf{B}}_k^C = \mathbf{B}_k^C - \mathbf{B}_k^C\mathbf{D}_{22_k}\mathbf{T}_k^{-1}\mathbf{D}_k^C, \tag{5.10}$$

$$\tilde{\mathbf{C}}_k^C = \mathbf{T}_k^{-1}\mathbf{C}_k^C, \tag{5.11}$$

$$\tilde{\mathbf{D}}_k^C = \mathbf{T}_k^{-1}\mathbf{D}_k^C, \tag{5.12}$$

where

$$\mathbf{T}_k = \mathbf{D}_k^C\mathbf{D}_{22_k} + \mathbf{I} \tag{5.13}$$

and $\mathbf{I}$ is the identity matrix.